RSC Advances

PAPER

View Article Online
View Journal | View Issue

Cite this: *RSC Adv.*, 2014, **4**, 19680

Characterization of hydroxyapatite deposition on biomimetic polyphosphazenes by time-of-flight secondary ion mass spectrometry (ToF-SIMS)†

Nicole L. Morozowich,‡ Jordan O. Lerach,‡ Tomasz Modzelewski,‡ Lauren Jackson, Nicholas Winograd* and Harry R. Allcock*

Received 2nd December 2013
Accepted 11th April 2014

DOI: 10.1039/c3ra47205a

www.rsc.org/advances

Synthetic bone grafts that promote the natural mineralization process are excellent candidates for the repair and replacement of bone defects. In this study, a series of phosphoester and phosphonic acid containing polyphosphazenes were examined for their ability to mineralize hydroxyapatite (HAp) during exposure to a solution of simulated body fluid (SBF) for a period of four weeks. Although all the polymers showed an initial mineralization response, the amount of deposition and the time scale were dependent upon the side group chemistry of the polymers. After exposure to SBF for one week, all polymers mineralized HAp. After three weeks in SBF, polymers containing phosphoester substituents showed no significant change, with a weight gain of <1%, while polymers containing phosphonic acid substituents underwent a significant increase in the amount of mineralized HAp, with weight gains between 5–10%. The morphology of mineralized features was observed with Environmental Scanning Electron Microscopy (ESEM). However, due to the structural complexity of the mineralized polymers, the identity of the mineralized phase could not be definitively identified using traditional characterization techniques such as energy dispersive spectroscopy (EDS), X-ray diffraction (XRD), Fourier-transform infrared spectroscopy (FTIR), or X-ray photoelectron spectroscopy (XPS). Time-of-flight secondary ion mass spectrometry (ToF-SIMS), a technique not previously explored for this type of application, successfully reveals details of the chemistry associated with the mineralized phase not possible to achieve with XRD analysis.

Introduction

More than 2.2 million bone graft procedures are performed worldwide.[1] The majority of these procedures rely on autografts and allografts, but due to their associated risks, a variety of synthetic bone grafts have been developed.[2] In order for the graft to be successful, it should match both the chemical and physical properties of bone.[3]

Several synthetic and natural polymers have been investigated for this application, including poly(lactic-*co*-glycolic acid) (PLGA),[4] poly(L-lactic acid) (PLA),[4–6] polycaprolactone (PCL),[4,7,8] bacterial cellulose,[9] chitosan,[10,11] and silk.[12] While many of these polymers show promising results, there are still a number of limitations preventing their use as implantable scaffolds. One of the main limitations is their lack of osteoinductive properties. Methods have been developed to improve these properties by means of incorporating growth factors[13] or other additives, such as autographic fillers and hydroxyapatite ($Ca_{10}(PO_4)_6(OH)_2$), into the polymer matrix by a physical mixing of the two components.[14–18] The incorporation of hydroxyapatite allows the materials to better mimic the chemical and physical properties of natural bone, as it comprises nearly 70 wt% of dry bone. Although the osteoinductive properties of these materials are enhanced, the mechanical properties suffer due to poor dispersion of the particles in the bulk polymer.[14,19]

One alternative to the use of particulate hydroxyapatite fillers to improve the osteoinductive properties of a material is to coat the sample with calcium phosphates, or to functionalize polymers with acidic (negatively charged) substituents to allow them to coordinate calcium and phosphate ions, thus promoting the mineralization of hydroxyapatite.[3,20,21] Many different types of polymers have been investigated for their ability to mineralize hydroxyapatite (HAp) using this method, and in most cases some type of biological apatite was deposited on the surface.[8,9,22] Studies have shown that these polymer scaffolds coated with hydroxyapatite had improved osteoinduction *in vivo*.[23,24] Moreover, these functional polymers should have better mechanical properties because of their ability to chemically bond to the hydroxyapatite.[25,26]

Traditional techniques used to characterize the mineralized phase rely heavily on scanning electron microscopy (SEM)

The Pennsylvania State University, Department of Chemistry, University Park, PA 16802, USA. E-mail: hra@chem.psu.edu; nxw@psu.edu

† Electronic supplementary information (ESI) available: Characterization data and hydrolysis profiles for all polymers examined along with ToF-SIMS quantification data for the mineralized polymers. See DOI: 10.1039/c3ra47205a

‡ These authors contributed equally to this manuscript.

coupled with energy dispersive spectroscopy (EDS), X-ray diffraction (XRD), and Fourier transform infrared spectroscopy (FTIR).[5,8,27] X-ray photoelectron spectroscopy (XPS) is also used but to a much lesser extent.[28] These techniques may be suitable for proper characterization of most polymer systems; however more complex systems may require alternative characterization methods, especially when the sample size is small and/or more than one phase is present on the sample.

An alternative analytical tool that is utilized to study such complex polymer systems is time-of-flight secondary ion mass spectrometry (ToF-SIMS). ToF-SIMS can provide excellent sensitivity, detecting attomolar concentrations for a variety of analytes,[29] as well as having the ability to generate chemical images of a surface with submicron spatial resolution. Chemical imaging capabilities can yield the location of specific analytes within a system. This is particularly advantageous in a situation where complementary ESEM images can be correlated. By collecting ToF-SIMS spectra over the same 2D array, the accurate location of specific features can be determined with chemical specificity. ToF-SIMS has been utilized previously for exceedingly complex systems, such as differentiation between multiple biologically-relevant apatite phases,[30] and for the chemical imaging of eukaryotic cells.[31,32] Furthermore, advancements in primary ion sources, specifically the shift towards cluster ions, such as C_{60}^+, allows researchers to investigate a multitude of sample varieties including both polymeric[33,34] and inorganic[35,36] substances, whereas, some atomic sources have proven much less effective.[37–39]

Recently, a number of polyphosphazene-based polymers have been developed and evaluated for their potential use in tissue engineering applications. Polyphosphazenes are tunable inorganic–organic hybrid polymers consisting of a backbone of alternating nitrogen and phosphorus atoms, with each phosphorus atom bearing two organic side groups.[40,41] The synthetic flexibility of this system has provided access to biocompatible and biodegradable polymers that show good osteocompatibility[42,43] both *in vitro*[44,45] and *in vivo*,[44–46] with little acute inflammatory response[47] and mineral deposition.[27] More recently, a number of phosphonic acid containing polyphosphazenes have been synthesized and characterized[48] in order to generate bioactive polymers capable of inducing *in situ* hydroxyapatite mineralization. In this work, their ability to mineralize hydroxyapatite from a simulated body fluid (SBF) solution was examined. The use of SBF to predict the *in vivo* bioactivity of a material has been well-established in the literature.[49]

Due to the complex nature of the mineralized polymers, their chemical composition was characterized by ToF-SIMS and morphologically by ESEM. As a means to confirm the presence of HAp detected by ToF-SIMS, XRD was used. To provide a unique and thorough characterization using ToF-SIMS, complete phase identification and relative quantification of HAp was accomplished using a QSTAR® XL ToF-MS which possesses both high mass accuracy and high mass resolution, while 2D chemical images that show distinct HAp localization were obtained on a Bio-ToF MS. With C_{60}^+ primary ion bombardment a number of characteristic and non-coincidental ions from HAp and the polymer are observed. Utilizing these ions as a marker, the location of HAp can be determined with chemical specificity, and in the case of the relative quantitation scheme, a relative amount of HAp within a sample. The identities of the HAp ions are confirmed with high mass resolution measurements and with MS/MS analyses. The information obtained identifies HAp features and the relative amounts on the surface of the samples.

Results and discussion

Polymer design

The polyphosphazenes used in this work were synthesized as previously described.[48] All polymers were designed with specific functional groups to meet three requirements: (1) spontaneous mineralization of HAp from a SBF solution, (2) bioerosion, and (3) high mechanical stability. The functional groups incorporated were: (1) phosphonic acid moieties due to their ability to coordinate calcium ions and promote HAp mineralization, (2) amino acid ester units to sensitize the polymers to hydrolysis, and (3) bulky aromatic units to provide polymer stiffness. Fig. 1 provides a representation of the chemical makeup of all polymers studied. Although the chemical structures seem similar, all of the polymers (**PEA**, **PEPA**, **PAA** and **PAPA**) have different properties which determine their mineralization behavior. For instance, polymers **PEA** and **PEPA** are hydrophobic with relatively high glass transition temperatures, and are soluble in chloroform and dimethylsulfoxide. Alternatively, polymers **PAA** and **PAPA** are hydrophilic with high glass transition temperatures, and are soluble in dimethylsulfoxide and methanol.

Mineralization experiments and composite characterization by ESEM

The polymers were tested for their mineralization behaviour using a dynamic treatment with 1.5× SBF for a period of four

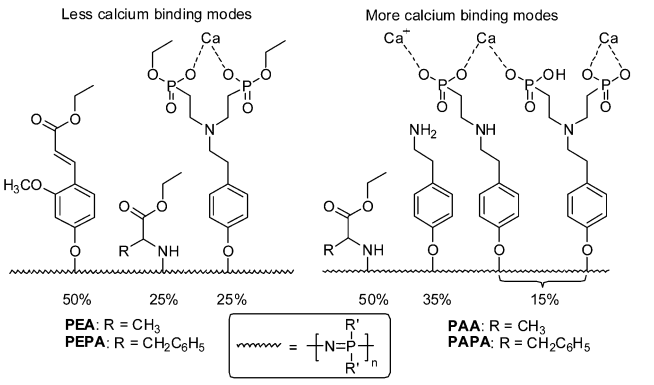

Fig. 1 Chemical composition of polymers studied, functionalized with phosphonic acid derivatives along with calcium binding modes available based on side group composition. The percentages listed represent the relative amounts of each side group attached to the polymer backbone and does not imply any regularity in the substitution pattern. (**PEA**: poly(PhosphoEster – Alanine)phosphazene, **PEPA**: poly(PhosphoEster – PhenylAlanine)phosphazene, **PAA**: poly(PhosphonicAcid – Alanine)phosphazene, **PAPA**: poly(PhosphonicAcid – Phenyl Alanine)phosphazene).

weeks. The SBF solution was exchanged daily for dynamic treatment and was utilized because it was found to be the most effective method of mineralization.[9] Also, a four week time period was chosen that should allow adequate time for mineralization to be observed. All polymers showed mineralization behaviour to some extent, with the final amount of apatite deposited dependent on the polymer and time immersed in solution. The lowest to highest amount of mineralized deposits occurred in the following order: **PEA** ≈ **PEPA** < **PAA** < **PAPA**.

When compared to the as-prepared clean sample which was not exposed to SBF, all of the polymers showed evidence of small inorganic crystalline deposits after 1 and 2 week exposure to SBF, as detected by ESEM and shown in Fig. 2, with all samples showing a heterogeneous distribution of particles along their surface. These samples were further analyzed using EDS. Calcium and phosphorus signatures were found for all mineralized samples using EDS, indicating that some type of apatite was present (Fig. 3A). However, the specific apatite phase was not determined by the Ca/P ratio due to the presence of phosphorus in the polyphosphazene backbone. Based on the tendency of dissolved phosphate ions to mineralize HAp because of their high chemical affinity for calcium ions,[50,51] coupled with HAp being the most thermodynamically stable phase precipitated from SBF under the conditions used,[52] HAp is the most likely candidate.

After 3 and 4 weeks in SBF, **PEA** and **PEPA** underwent no significant changes from the results at weeks 1 and 2. However, **PAA** and **PAPA** showed a strikingly different behavior, with 3 morphologies of mineral deposits detected on their surfaces. The first deposit type was the same as those observed at weeks 1 and 2, with small inorganic deposits distributed homogeneously on the surface. The second and third were clusters of inorganic deposits distributed heterogeneously across the surface, with one cluster type possessing an irregular shape and the other exhibiting a globular morphology. Using EDS, both clusters were found to be apatite phases showing intense calcium signatures, and were probably the same phase, but in two different morphologies. The morphology of both the globular clusters[22,27,53] and the irregularly-shaped clusters[7,54] have been identified as HAp in previous literature reports. This behavior was not found for **PEA** and **PEPA**, which is a direct result of the difference in side group chemistry, shown in Fig. 1. Because the mineralization process begins with the initial binding of calcium ions to the free phosphonic acid groups, the availability of these groups to the SBF solution becomes the limiting factor, and ultimately determines the mineralization behaviors.[3,53] Based on this, **PAA** and **PAPA** which contain phosphonic acid substituents with six P-OH groups per site available for calcium binding, should perform better than **PEA** and **PEPA** which contain phosphoester derivatives that contain only two free P-OH groups per site available for calcium binding. An increase in the number of P-OH linkages increases the number of binding modes available to calcium, thus increasing the probability of mineralization. This hypothesis is supported by the weight gain data provided in the following section. The presence of HAp was later confirmed by ToF-SIMS

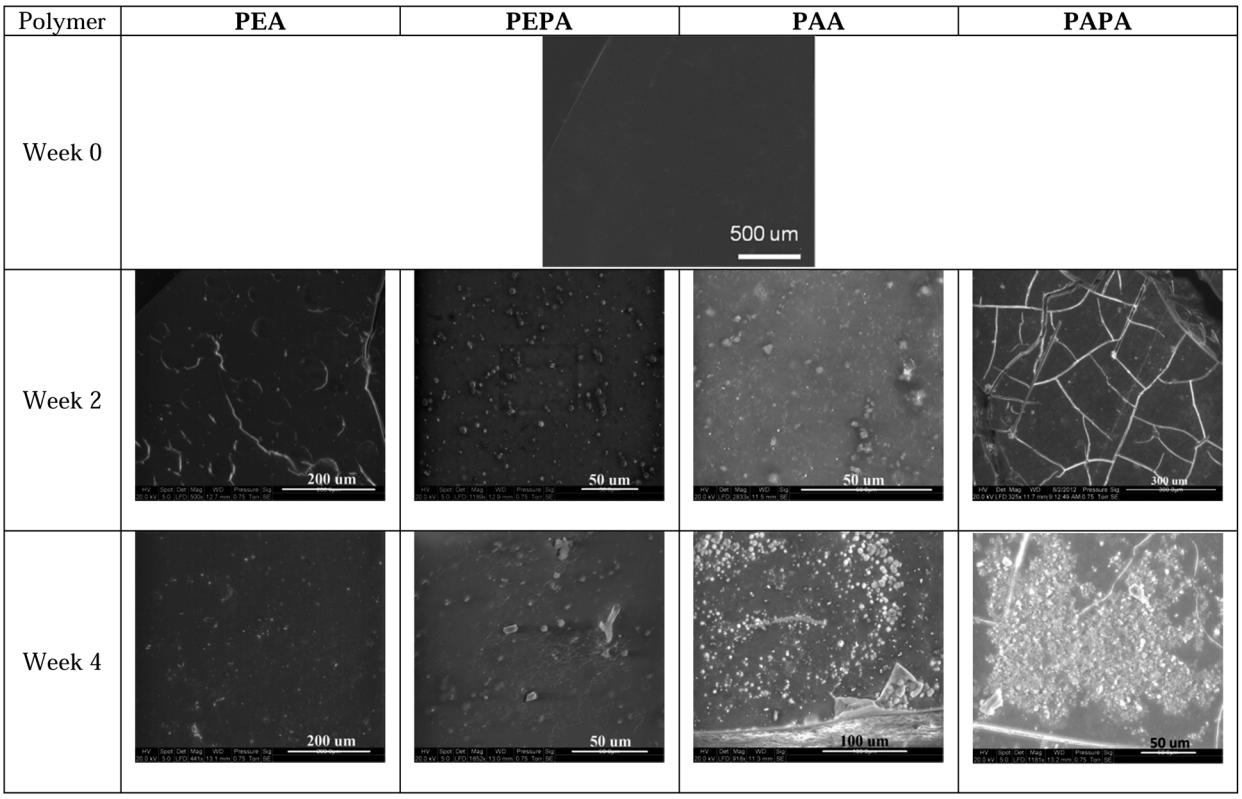

Fig. 2 ESEM images of polymer samples before mineralization (clean **PEA** film shown as a representative of all polymers), and after 2 and 4 weeks exposure to simulate body fluid (SBF).

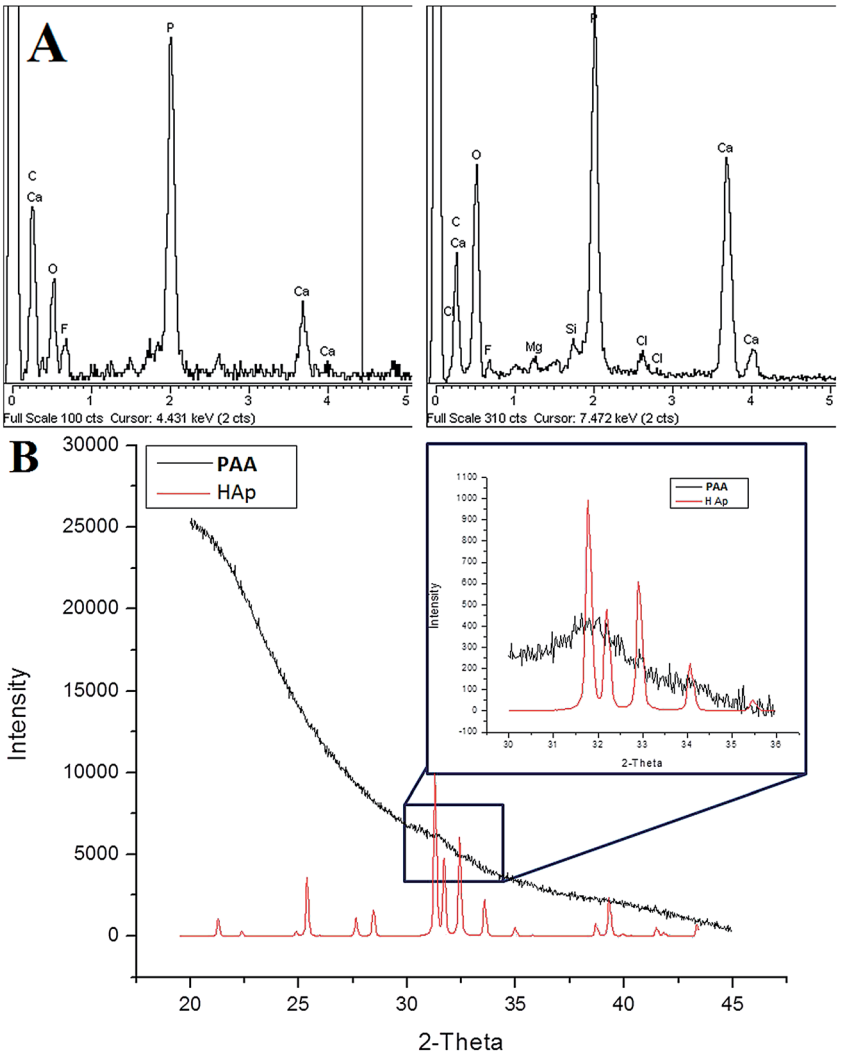

Fig. 3 (A) An EDS spectrum obtained for **PEA** (left), showing calcium phosphate deposition after 1 week exposure (similar spectra were obtained for all polymers during first 2 weeks, and for **PEA** and **PEPA** at weeks 3 and 4), along with an EDS spectrum of **PAPA** (right) after 4 week treatment with SBF. (B) An XRD pattern of **PAA** after 4 weeks exposure to SBF.

and XRD. To date, this is the first reported, fully characterized polyphosphazene that mineralized HAp from SBF.

Weight gain after mineralization in SBF

All polymers were tested for their weight gain after exposure to SBF. Pre-weighed samples of the polymers were immersed in an SBF solution which was exchanged daily. After each week three samples were removed, rinsed with de-ionized water, and lyophilized. The then-dry samples were re-weighed to determine the additional mass gain from the apatite deposits before further analysis by ESEM, ToF-SIMS, and XRD. All mass changes were normalized to the percent mass loss due to hydrolysis, which was estimated from exposure of the polymer to a solution of phosphate buffered saline (PBS), also exchanged daily. The results are shown in Fig. 4. **PAA** and **PAPA** gained the most weight, with approximately 4.5 and 10% weight gains, respectively, while **PEA** and **PEPA** had less than 1% weight gain.

ToF-SIMS findings

The similarity in the chemical makeup of the polymer to HAp causes unreliability with characterization methods such as EDS, FTIR, and XPS. The phosphate unit is present in both the polymer and HAp, and it would be impossible to differentiate the source of the signal, thus complicating the chemical characterization of the mineralized polymers. Furthermore, XRD data (Fig. 3B) provides some chemical evidence for HAp formation, but the highly amorphous nature of the polymer masks most of the diffractions for HAp.

With C_{60}^{+} primary ion bombardment, a large number of characteristic, non-coincidental ions from HAp and the polymer are detected from the collected spectra. This diversity in ion identity allows for the differentiation of HAp ions due to any number of characteristic ions that cannot be generated from the polymeric species. The ion identities were compared to HAp reference material and ions $[CaO]^{+}$, $[Ca_2O]^{+}$, $[Ca_2O_2]^{+}$, $[Ca_2PO_3]^{+}$, $[Ca_2PO_4]^{+}$, $[Ca_3PO_5]^{+}$, and $[Ca_4PO_6]^{+}$ well represent the HAp

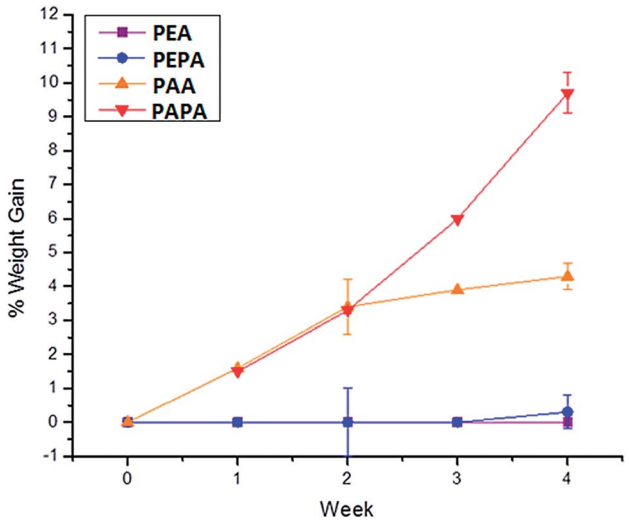

Fig. 4 Percent weight gain of apatite for all polymers studied, upon exposure to SBF for 4 weeks.

moiety. Also, polymeric samples which had no exposure to SBF yielded characteristic ions of $[C_7H_7]^+$ and $[C_6H_5]^+$ due to fragmentation of the functionalized polymer side-groups. Furthermore, identification is aided by utilizing instrumentation which possess high mass accuracy and tandem MS capabilities (Fig. 6). It should be noted that polydimethylsiloxane (PDMS) was also detected at the surface of all polymers. The most intense ions in the polymer spectra at *m*/*z* 73 and 147 are due to PDMS contamination. In light of this information the characteristic ions chosen to represent the polyphosphazenes and HAp phase are non-isobaric with the PDMS ions. It was found that solvent washes in hexanes diminish the PDMS signal from the polymer surface (ESI†). Given the current capabilities of ToF-SIMS instruments, chemical images can be created using mass spectra obtained at various points across a sample, allowing for the generation of a 2D representation of the distribution of analytes on a sample (Fig. 5). Also, by examining the relative ion signal strength among a group of samples, the amount of HAp present at each time point may be relatively quantified (Fig. 7).

Imaging work was performed on a Bio-ToF mass spectrometer.[55] Control spectra for HAp and of the unexposed polymers were analyzed and compared to identify unique, abundant ions for both species.

PAA and **PAPA** were examined first since they showed evidence for the most apatite deposition by ESEM and weight gain analyses. Spectra were obtained for **PAA** and **PAPA** after mineralization in SBF for 1, 2, 3, and 4 weeks. Before ToF-SIMS imaging analysis, the mineralized samples were mapped using ESEM due to the heterogeneous deposition of HAp. By imaging the entire sample with ESEM, the HAp regions were identified, and then samples with abundant HAp localization were subsequently transferred to the mass spectrometer. Analysis of the pre-mapped ESEM samples allowed a comparison of the ToF-SIMS images with the ESEM images, to allow chemical identification of coincidental features. The HAp had characteristic peaks at *m*/*z* 56, 96, 112, 159, 175, 231, and 287 which

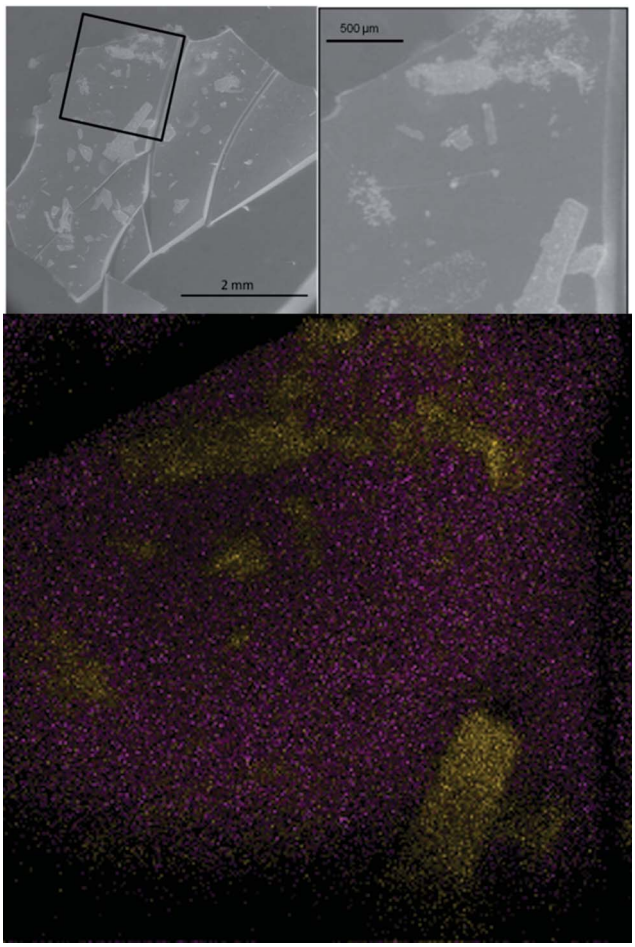

Fig. 5 (Top left and right) ESEM images of **PAA** at week 3. (Bottom) ToF-SIMS of the same region. Yellow pixels in the SIMS image represent the characteristic HAp ions and purple represents the characteristic polymer ions.

were assigned as $[CaO]^+$, $[Ca_2O]^+$, $[Ca_2O_2]^+$, $[Ca_2PO_3]^+$, $[Ca_2PO_4]^+$, $[Ca_3PO_5]^+$, and $[Ca_4PO_6]^+$ respectively. The polymer had unique ions at *m*/*z* 77 and 91 which are indicative of the $[C_6H_5]^+$ and $[C_7H_7]^+$ ions. These unique identifiers allow characterization of complex samples.

After analysis, the intensities of the ions listed for HAp and the polymer were utilized to generate 2D chemical images. Mass spectra were collected over a 2008 × 2008 µm^2 field-of-view (FOV) for **PAA** and **PAPA** at before and after exposure to SBF for 2 and 4 weeks, where the peaks previously mentioned were used to create the 2D images. The integrated intensity for the mass spectra at each pixel in a 256 × 256 array was summed together for each respective ion, then the intensities were summed together for each pixel. The 2D chemical image for **PAA** showing the HAp signal as yellow pixels and polymer in purple is compared to the same area analyzed by ESEM in Fig. 5. The figure clearly shows localization of the HAp signal to the surface features on the polymer in the ESEM images. Analysis of other polymer samples shows no distinguishable surface features after 1 and 2 weeks of SBF exposure. However, in samples with 3 to 4 weeks of SBF exposure surface features

were observed. This localization is believed to be a consequence of the PDMS detected which would have changed the surface chemistry based on the local PDMS content, allowing only portions of the sample to effectively interact with the SBF and coordinate the necessary ions to allow for the growth of HAp on the surface.

Confirmatory results which differentiate HAp signal from the polymer signal are shown in Fig. 6. In this figure mass spectra from regions of interest of the provided SIMS image (Fig. 5 bottom) of **PAA** week 3 are exhibited. In Fig. 6 (bottom) characteristic mass regions of the HAp feature are plotted along with HAp reference material. In Fig. 6 (top) exposed polymer regions are plotted with **PAA** reference before and after hexane washes, which show an increase in the characteristic $[C_7H_7]^+$ and $[C_6H_5]^+$ fragments. Full spectra and highlighted regions of interest are provided in the supporting materials. From these spectra the ion signatures from each region uniquely identify HAp compared to polymeric regions allowing for differentiation based on ion signatures.

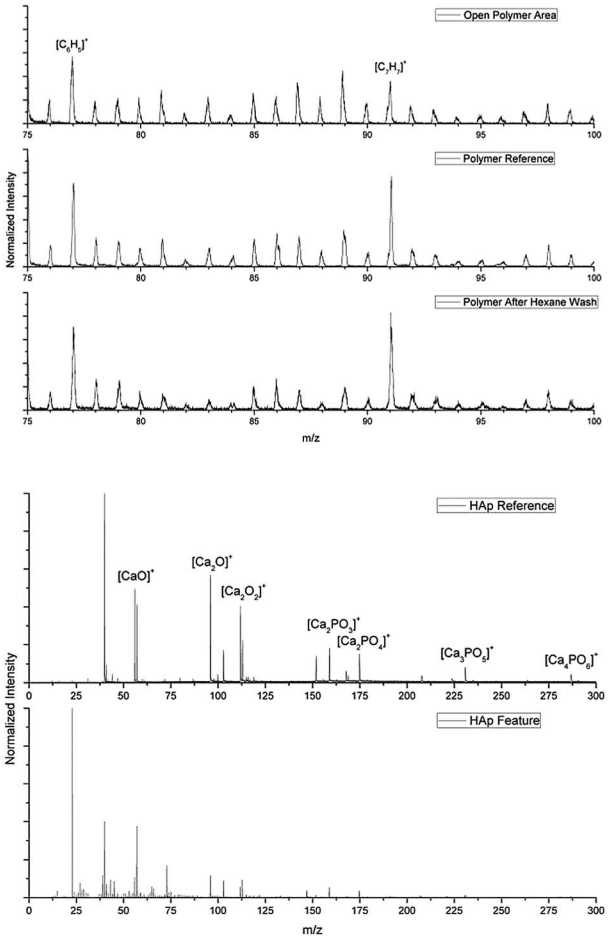

Fig. 6 Select polymer region compared to PAA reference and PAA reference after triplicate hexane washes (top). Select regions of mass spectra from regions of interest from PAA week 3 for HAp feature as compared to HAp reference (bottom). Characteristic ions are observed in the respective spectra. Complete spectra and region of interest are presented in ESI.†

As shown in Fig. 6, there is a direct overlap between the HAp phase detected by ToF-SIMS and the surface features observed by ESEM. The areas of high electron density in the ESEM images correlate in the ToF-SIMS image to HAp (yellow). The chemical image provided for polymer **PAA** at week 3 provides clear evidence for HAp mineralization. However, identification of HAp after 1 and 2 weeks mineralization in SBF for polymers **PAA** and **PAPA** was not possible using the Bio-ToF due to low or no HAp signal detected.

The signal to noise ratio for the ToF-SIMS spectra obtained for **PAA** and **PAPA** after 1 and 2 weeks of SBF treatment was not sufficient to distinguish background from small quantities of HAp. To overcome this limitation the samples were analyzed using a QSTAR® XL triple quadrupole ToF-MS modified with a 20 keV C_{60}^+ primary ion source to enable SIMS analysis. This system possesses higher mass accuracy (10 ppm) and mass resolution ($m/\Delta m$ > 12 000) than the Bio-ToF instrument albeit with less reliable imaging capabilities. Empirical masses were compared to their calculated exact mass values and their subsequent assignments verified.

Because the exact masses of several ions that relate to HAp were identified and separated from interfering signals, a relative quantitation study was performed to determine the amount of HAp deposition as a function of exposure to SBF. The abundance of several HAp ions were compared and all were found to increase in intensity during the exposure time to SBF.

Relative quantitation data are shown in Fig. 7 for the $[Ca_2O_2]^+$, $[Ca_2PO_3]^+$, $[Ca_2PO_4]^+$ and $[Ca_4PO_6]^+$ ions. The overall trend is toward an increase in HAp signal compared to each individual group. These results support the weight gain data (Fig. 4), which showed a progressive increase in the weight of the samples with increasing exposure time to SBF. It also supports the data presented in Fig. 2, where **PAA** and **PAPA** mineralized significantly more HAp than **PEA** and **PEPA**.

The magnitude of the standard deviation is not surprising considering the heterogeneous deposition of HAp on the polymer surface, as shown by SIMS and ESEM imaging. Also, SIMS relative quantitation can be accomplished more readily on samples with a lower surface roughness[56] than that observed for the mineralized samples. Despite this, an increase in the HAp

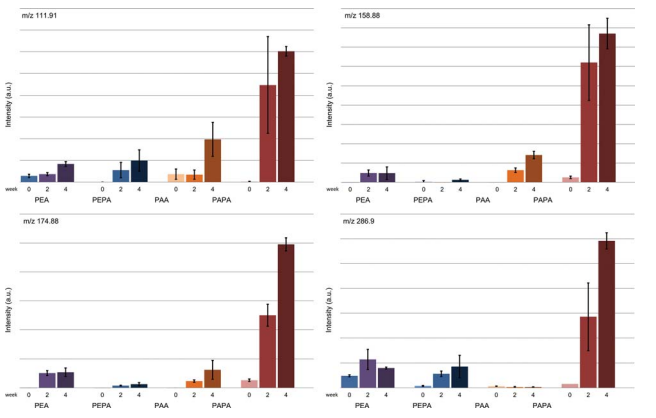

Fig. 7 Relative quantitation trends of some HAp ions observed in the QSTAR® XL.

signal as a function of SBF exposure time for each polymer was clearly established. In some instances, the specific ion signal was detected before SBF exposure, but was attributed to be background noise.

Phase confirmation of mineralized polymers by XRD

Following ESEM evaluation, all polymers were characterized by XRD to confirm the identity of the nucleated apatite from SBF. The XRD patterns of polymers **PEA** and **PEPA** before and after mineralization were identical, with no observable signal for HAp. They both contained two predominant amorphous peaks centered at $2\theta = 5.21^\circ$ and 21.36° (not shown). Thus, there was not enough of the mineralized phase present. These results were in accordance with the observed weight gain of less than 1%.

XRD patterns of polymers **PAA** and **PAPA** were also obtained before and after mineralization. Before mineralization, both polymers contained two predominant amorphous peaks centered at $2\theta = 6.87^\circ$ and 19.26°. After incubation in SBF for 1 and 2 weeks, the XRD patterns did not change, even though mineralized deposits were detected on their surface by ESEM. However, after incubation in SBF for 3 and 4 weeks, a new peak appeared at $2\theta = 31.7^\circ$, as shown in Fig. 3B. The reflection at 31.7° (211) is characteristic of the strongest reflection from hydroxyapatite [HAp, $Ca_{10}(PO_4)_6(OH)_2$, FIZ 97849, major $2\theta = 31.7^\circ$ (211 *hkl*), 32.2° (112 *hkl*), and 32.9° (300 *hkl*)]. Like many examples in the literature, the 2θ peaks for nucleated HAp are broad.[6–8,22] For example, the three intense peaks for HAp listed above usually appear as one broad peak, centered at 31.7°, representing nano-crystalline HAp.[57]

Materials and methods

Reagents and equipment for polymer synthesis

All synthesis reactions were carried out using standard Schlenk line techniques and a dry argon atmosphere. The glassware was dried overnight in an oven at 125 °C before use. Diethylvinylphosphonate,[58] boc-tyramine,[59] and ethyl ferulate[60] were synthesized following previously reported procedures. The synthesis of bis-(diethyl phosphonate)-*N*,*N*-diethyltyramine (**DPT**), (diethyl phosphonate)-*N*-ethyltyramine (**MPT**), bis-(phosphonic acid)-*N*,*N*-diethyltyramine (**DPAT**), and (phosphonic acid)-*N*-ethyltyramine (**MPAT**) is described in an earlier publication.[48] Poly(dichlorophosphazene) was prepared by the thermal ring-opening polymerization of recrystallized and sublimed hexachlorocyclotriphosphazene (Fushimi Chemical Company, Japan or Ningbo Chemical, China) in evacuated Pyrex tubes at 250 °C.[41] ^{31}P and ^{1}H NMR spectra were obtained with a Bruker 360 WM instrument operated at 145 MHz and 360 MHz, respectively. ^{31}P shifts are reported in ppm relative to 85% H_3PO_4 at 0 ppm. Glass transition temperatures were measured with a TA Instruments Q10 differential scanning calorimetry apparatus with a heating rate of 10 °C min^{-1} and a sample size of *ca.* 10 mg. Gel permeation chromatography was performed using a Hewlett-Packard 1047A refractive index detector and two Phenomenex Phenogel linear 10 columns. The samples were eluted at 1.0 mL min^{-1} with a 10 mM solution of tetra-*n*-butylammonium nitrate in THF. The elution times were calibrated with polystyrene standards. Water contact angle measurements were obtained using a Rame'-Hart contact angle goniometer. Images were produced with "Snappy" video and analyzed using Image J.

Polymer synthesis and hydrolysis

The synthesis, characterization, and hydrolysis behavior of all polymer was reported previously.[48] Characterization data are provided in the ESI.†

Preparation of simulated body fluid solution

A 1.5× SBF solution was prepared following the procedure reported by Kokubo *et al.*[61] Briefly, analytical grade NaCl, $NaHCO_3$, KCl, $K_2HPO_4 \cdot H_2O$, $MgCl_2 \cdot 6H_2O$, 1 M HCl, $CaCl_2$, and Na_2SO_4 were added sequentially to de-ionized water and buffered to a pH of 7.25 with THAM. The final concentrations of ionic species (in mM) was 213 Na^+, 7.5 K^+, 2.3 Mg^{2+}, 3.8 Ca^{2+}, 221.7 Cl^-, 6.3 HCO_3^-, 1.5 HPO_4^-, and 0.8 SO_4^{2-}. The solution was stored at 5 °C before use.

Mineralization of polymers in SBF

Individual polymers were dissolved in dimethylsulfoxide (2.5 wt/v %) and solution cast into films (6 cm × 2.5 cm). Solvent was removed by lyophilization, followed by storage under vacuum for one week. To obtain the initial mineralization response the experiment was carried out on a small scale by dividing the films into 8 samples (~15 mg each) and placing them in 7.5 mL SBF. The samples were maintained in a shaker bath at 37 °C for 4 weeks, with a daily exchange of the SBF solution. Two samples were removed every week for each polymer, rinsed with de-ionized water several times, and dried by lyophilization. After the small scale experiment, a larger scale experiment was conducted by dividing the films into 4 samples (~50 mg each) and placing them in 20 mL of SBF. The samples were maintained in a shaker bath at 37 °C for 4 weeks, with a daily exchange of the SBF solution. Two samples were removed every two weeks for each polymer, rinsed with de-ionized water several times, and dried by lyophilization.

Equipment for the characterization of polymer–apatite composites

The samples obtained from SBF were analyzed by the methods described below.

Morphology by ESEM. The morphology was determined by environmental scanning electron microscopy (ESEM). Images were obtained using a Phillips REI Quanta 200 ESEM. Low vacuum mode was used for imaging uncoated samples under the following conditions: 20 keV source voltage, pressure of 0.68 Torr, and a working distance of 12 mm. Energy dispersive spectroscopy (EDS) was performed to determine the presence of calcium utilizing an Oxford EDS attachment and analyzed using INCA software. The Ca/P ratio was not calculated due to the polymer itself containing phosphorus.

Phase identification and 2D chemical imaging using a Bio-ToF SIMS instrument. Chemical-imaging analyses were carried out on a ToF-SIMS instrument previously described in detail.[55]

In brief, an IOG-C60 C_{60}^+ (Ionoptika, Southampton, UK) primary ion source was utilized on a pulsed extraction SIMS instrument. The primary ion gun used produced a 40 keV C_{60}^+ 50 ns pulsed primary ion beam of 50–125 pA for sample interrogation. The ToF-SIMS instrument utilized pulsed extraction at +2500 V stage bias and mass discrimination with a dual-stage reflectron. The primary ion beam was rastered across the sample in a 2008 × 2008 μm^2 area while collecting spectra at each pixel in a 256 × 256 array. A total of 30 spectra per pixel were obtained to generate chemical images. The Bio-ToF mass spectrometer is capable of reaching mass resolution of $m/\Delta m$ of 5000, however the height of the samples varied greatly over the acquisition areas which caused a severe decrease in mass resolution. The total primary ion dose at the sample surface (<1 × 10^{10} C_{60}^+ cm^{-2}) was well below the static limit so no interference from chemical damage is visible. Control spectra were obtained for the HAp phase and compared to the polymer-based samples. A series of masses unique to the polymer and HAp phase that were distinguishable from the background signal were chosen. Polymer ions chosen were at m/z 77 and 91. The HAP ions chosen were at m/z 56, 96, 112, 159, 175, 231 and 287 and their identities are verified by high mass resolution measurements on the QSTAR® XL.

High Mass Resolution and Accuracy ToF-MS and Relative Quantitation with QSTAR® XL ToF-SIMS Instrument. The QSTAR® XL (Applied Biosystems/MDS Sciex) was modified in-house to incorporate a 20 keV C_{60}^+ source (Ionoptika Ltd.) for SIMS analysis.[62,63] The QSTAR® XL system is a tandem quadrupole orthogonal time-of-flight mass spectrometer. For all aforementioned samples, an approximately 15 pA current beam of C_{60}^+ was produced by a 20 keV Ionoptika C_{60}^+ source operated in direct current mode. The relative quantitation scheme was adapted from previously reported research[56] and briefly described here, as used on the QSTAR®XL system. While collecting each surface spectrum, the sample stage was rastered continuously across the surface of the samples in 10 μm steps. The samples used for analysis each had a surface area of approximately 5 × 5 mm^2. Three trials for each polymer at each time point were collected. For each trial, 180 successive scans were collected by multi-channel acquisition, thus, all aforementioned scans are summed in a running total of intensities from the first to the last scan. Each multi-channel acquisition scan lasted 0.33 seconds. Peak assignments are determined with <10 ppm accuracy. The average intensity and the standard deviation of the three trials per sample are calculated to enable a more accurate and precise measurement of the yield of the ions of interest from each sample.

Phase Identification by XRD. The mineral phase was determined by X-ray diffraction (XRD). XRD patterns were collected using a PANalytical X-Pert Pro MPD Theta–Theta goniometer with Cu-Kα radiation, and fixed slit incidence (0.25 deg. divergence, 0.50 deg. anti-scatter, specimen length 10 mm) and diffracted (0.25 deg. anti-scatter, 0.02 mm nickel filter) optics. Samples were prepared by flattening the mineralized film onto a zero background holder using a glass slide. Data were collected at 45 kV and 40 mA from 5–50 deg. 2θ using a PIXcel detector in scanning mode with a PSD length of 3.35 deg. 2θ and 255 channels for a duration time of ~20 minutes. The resulting patterns were analyzed with Jade+9 software and compared to patterns found in the International Center for Diffraction Data (ICDD) database and the Inorganic Crystal Structure Database (ICSD). The percent weight gain of the mineralized phase was determined by weighing samples before and after mineralization. Each sample was normalized using the weight lost obtained from the phosphate buffered saline specimens.

Conclusions

A series of phosphoester and phosphonic acid polyphosphazenes were examined for their bone-bonding ability in real-time when exposed to SBF containing near physiological ion concentrations. The final results show a clear dependence on the side group chemistry of the different polymers. During the four week period, phosphoester containing polymers (**PEA** and **PEPA**) show a minimal HAp mineralization response, with a total weight gain of less than 1%, whereas the phosphonic acid polymers (**PAA** and **PAPA**) have a much greater response, with ~4.5–10% weight gain by week 4. Due to the complex nature of the mineralized polymers, ToF-SIMS was the primary method of HAp characterization. The Bio-ToF mass spectrometer was used for 2D chemical imaging and phase identification whereas the modified QSTAR®XL mass spectrometer modified for ToF-SIMS was used for phase identification and relative quantification of HAp. ESEM and XRD were used to support the ToF-SIMS results. This is the first report showing the utility of ToF-SIMS to characterize a type of apatite deposited onto a polymer substrate. This method provides another means of characterization when existing methods such as XRD, FTIR, and EDS prove insufficient. **PAPA** is an excellent candidate for an implantable bone graft, not only for its ability to nucleate HAp, which will increase the polymers osteoconductivity and osteoinductivity, but for its ability to hydrolyze at a similar rate to HAp mineralization. Thus providing the cavities necessary to mineralize throughout the entire graft, while also maintaining the mechanical stability required.

Acknowledgements

The authors acknowledge financial support from the Department of Energy under Grant DE-FG02-06ERER158063.

Notes and references

1 P. V. Giannoudis, H. Dinopoulos and E. Tsiridis, *Injury*, 2005, **36**, S20–S27.
2 C. T. Laurencin and Y. Khan, *Bone Graft Substitute Materials,* http://emedicine.medscape.com/article/1230616-overview, 2009.
3 N. M. Alves, I. B. Leonor, H. S. Azevedo, R. L. Reis and J. F. Mano, *J. Mater. Chem.*, 2010, **20**, 2911–2921.
4 J. C. Middleton and A. K. Tipton, *Biomaterials*, 2000, **21**, 2335–2346.
5 Q. Cai, Q. Xu, Q. Feng, X. Cao, X. Yang and X. Deng, *Appl. Surf. Sci.*, 2011, **257**, 10109–10118.

6 R. Zhang and P. X. Ma, *J. Biomed. Mater. Res.*, 1998, **45**, 285–293.
7 C. Choong, S. Yuan, E. S. Thian, A. Oyane and J. Triffitt, *J. Biomed. Mater. Res., Part A*, 2012, **100**, 353–361.
8 D. O. Costa, B. A. Allo, R. Klassen, J. L. Hutter, S. J. Dixon and A. S. Rizkalla, *Langmuir*, 2012, **28**, 3871–3880.
9 K. A. Zimmerman, J. M. LeBlanc, K. T. Sheets, R. W. Fox and P. Gatenholm, *Mater. Sci. Eng., C*, 2011, **31**, 43–49.
10 X. Wang, J. Ma, Q. Feng and F. Z. Cui, *Biomaterials*, 2002, **23**, 4591.
11 X. Wang, J. Ma, Y. Wang and B. He, *Biomaterials*, 2001, **22**, 2247.
12 B. B. Mandal, A. Grinberg, E. S. Gil, B. Panilaitis and D. L. Kaplan, *Proc. Natl. Acad. Sci. U. S. A.*, 2012, **109**, 7699–7704.
13 K. W.-H. Lo, K. M. Ashe, H. M. Kan and C. T. Laurencin, *Regener. Med.*, 2012, **7**, 535–549.
14 H. Liu and T. J. Webster, *Int. J. Nanomed.*, 2010, **5**, 299–313.
15 S. P. Nukavarapu, S. G. Kumbar, J. L. Brown, N. R. Krogman, A. L. Weikel, M. D. Hindenlang, L. S. Nair, H. R. Allcock and C. T. Laurencin, *Biomacromolecules*, 2008, **9**, 1818–1825.
16 P. Q. Ruhe, E. L. Hedberg-Dirk, N. T. Padron, P. H. M. Spauwen, J. A. Jansen and A. G. Mikos, *Tissue Eng.*, 2006, **12**, 789–800.
17 Y. Wang, L. Liu and S. Guo, *Polym. Degrad. Stab.*, 2010, **95**, 207–213.
18 *Fundamental Biomechanics for Bone Tissue Engineering*, ed. X. Wang, J. S. Nyman, H. Leng, X. Dong and M. Reyes, Morgan and Claypool, 2010.
19 S. E. Kim, H. W. Choi, H. J. Lee, J. H. Chang, J. Choi, K. J. Kim, H. J. Lim, Y. J. Jun and S. C. Lee, *J. Mater. Chem.*, 2008, **18**, 4994–5001.
20 I. B. Lenor, H. S. Azevedo, C. M. Alves and R. L. Reis, in *Biodegradable systems in tissue engineering and regenerative medicine*, ed. R. L. Reis and J. S. Roman, CRC Press, Boca Raton, Florida, 2006, pp. 223–235.
21 A. L. Oliveria and R. L. Reis, in *Biodegradable systems in tissue engineering and regenerative medicine*, ed. R. L. Reis and J. S. Roman, CRC Press, Boca Raton, Florida, 2005, pp. 205–221.
22 A. Phadke, C. Zhang, Y.-S. Hwang, K. Vecchio and S. Varghese, *Biomacromolecules*, 2010, **11**, 2060–2068.
23 A. Bigi, M. Fini, B. Bracci, E. Bonanini, P. Torricelli, G. Giavaresi, N. N. Aldini, A. Facchini, F. Sbaiz and R. Giardino, *Biomaterials*, 2008, **29**, 1730–1736.
24 Y. S. Pek, S. Gao, M. S. Arshad, K. J. Leck and J. Y. Ying, *Biomaterials*, 2008, **29**, 4300–4305.
25 B. Fu, X. M. Sun, W. X. Qian, Y. Q. Shen, R. R. Chen and M. Hannig, *Biomaterials*, 2005, **26**, 5104–5110.
26 X. Wang, J. Ma, Y. Wang and B. He, *Biomaterials*, 2001, **22**, 2247–2255.
27 N. L. Morozowich, J. L. Nichol and H. R. Allcock, *Chem. Mater.*, 2012, **24**, 3500–3509.
28 M. P. Casaletto, S. Kaciulis, A. Mezzi, L. Ambrosio and F. Branda, *Surf. Interface Anal.*, 2002, **34**, 45–49.
29 R. M. Braun, J. Cheng, E. E. Parsonage, J. Moeller and N. Winograd, *Anal. Chem.*, 2006, **78**, 8347–8353.
30 H. B. Lu, C. T. Campbell, D. J. Graham and B. D. Ratner, *Anal. Chem.*, 2000, **72**, 2886–2894.
31 J. S. Fletcher, S. Rabbani, A. Henderson, N. P. Lockyer and J. C. Vickerman, *Rapid Commun. Mass Spectrom.*, 2011, **25**, 925–932.
32 F. Benabdellah, A. Seyer, L. Quinton, D. Touboul, A. Brunelle and O. Laprévote, *Anal. Bioanal. Chem.*, 2010, **396**, 151–162.
33 X. Ren, L.-T. Weng, C.-M. Chan and K.-M. Ng, *Anal. Chem.*, 2012, **84**, 8497–8504.
34 H. Moon, D. Wells and J. Gardella Jr, *J. Am. Soc. Mass Spectrom.*, 2012, **23**, 23–29.
35 T. M. Brewer and L. T. Demoranville, *Anal. Methods*, 2012, **4**, 3491–3496.
36 A. Tognazzi, A. M. Dattilo, L. Bracchini, M. Aggravi, F. Benetti, E. Mugnaini, A. Magnani and C. Rossi, *Surf. Interface Anal.*, 2011, **43**, 1108–1119.
37 R. M. Braun, J. Cheng, E. E. Parsonage, J. Moeller and N. Winograd, *Anal. Chem.*, 2006, **78**, 8347–8353.
38 A. M. Piwowar and J. C. Vickerman, *Surf. Interface Anal.*, 2010, **42**, 1387–1392.
39 A. M. Piwowar, N. Lockyer and J. C. Vickerman, *Appl. Surf. Sci.*, 2008, **255**, 912–915.
40 H. R. Allcock, *Chemistry and Applications of Polyphosphazenes*, John Wiley and Sons, Hoboken, 2003.
41 H. R. Allcock and R. L. Kugel, *J. Am. Chem. Soc.*, 1965, **87**, 4216.
42 N. R. Krogman, A. L. Weikel, K. A. Kristhart, S. P. Nukavarapu, M. Deng, L. S. Nair, C. T. Laurencin and H. R. Allcock, *Biomaterials*, 2009, **30**, 3035–3041.
43 A. L. Weikel, S. G. Owens, N. L. Morozowich, M. Deng, L. S. Nair, C. T. Laurencin and H. R. Allcock, *Biomaterials*, 2010, **31**, 8507–8515.
44 M. Deng, L. S. Nair, S. P. Nukavarapu, S. G. Kumbar, T. Jiang, N. R. Krogman, A. Singh, H. R. Allcock and C. T. Laurencin, *Biomaterials*, 2008, **29**, 337–349.
45 S. G. Kumbar, S. Bhattacharyya, S. P. Nukavarapu, Y. M. Khan, L. S. Nair and C. T. Laurencin, *J. Inorg. Organomet. Polym. Mater.*, 2006, **16**, 365–385.
46 S. Sethuraman, L. S. Nair, S. El-Amin, R. Farrar, M.-T. N. Nguyen, A. Singh, H. R. Allcock, Y. E. Greish, H. R. Brown and C. T. Laurencin, *J. Biomed. Mater. Res., Part A*, 2006, **77**, 679–687.
47 M. Deng, L. S. Nair, S. P. Nukavarapu, T. Jing, W. A. Kanner, X. Li, S. G. Kumbar, A. L. Weikel, N. R. Krogman, H. R. Allcock and C. T. Laurencin, *Biomaterials*, 2010, **31**, 4898–4908.
48 N. L. Morozowich, T. Modzelewski and H. R. Allcock, *Macromolecules*, 2012, **45**, 7684–7691.
49 T. Kokubo and H. Takadama, *Biomaterials*, 2006, **27**, 2907–2915.
50 S. Suzuki, M. R. Whittaker, L. Grondahl, M. J. Monteiro and E. Wentrup-Byrne, *Biomacromolecules*, 2006, **7**, 3178–3187.
51 M. Tanahasha and T. Matsuda, *J. Biomed. Mater. Res.*, 1997, **34**, 305–315.
52 S. V. Dorozhkin and M. Epple, *Angew. Chem., Int. Ed.*, 2002, **41**, 3130–3146.

53 T. Kokubo, H. M. Kim and M. Kawashita, *Biomaterials*, 2003, **24**, 2161–2175.
54 M. Kawashitaa, M. Nakaoa, M. Minodab, H.-M. Kima, T. Beppud, T. Miyamotoe, T. Kokuboa and T. Nakamuraf, *Biomaterials*, 2003, **24**, 2477–2484.
55 R. M. Braun, P. Blenkinsopp, S. J. Mullock, C. Corlett, K. F. Willey, J. C. Vickerman and N. Winograd, *Rapid Commun. Mass Spectrom.*, 1998, **12**, 1246–1252.
56 L. M. Jackson, J. J. Hue and N. Winograd, *Surf. Interface Anal.*, 2013, **45**, 237–239.
57 A. R. Bushroa, R. G. Rahbari, H. H. Masjuki and M. R. Muhamad, *Vacuum*, 2012, **86**, 1107–1112.
58 P. Fourgeaud, C. Midrier, J.-P. Vors, J.-N. Volle, J.-L. Pirat and D. Virieux, *Tetrahedron*, 2010, **66**, 758–764.
59 B. Anders, H. Patrik, J. Robert, L. Lanna, L. A. Eva-Lotte, S. Pernilla, S. Marianne, W. Lars and M. Kay, *World Intellectual Property Organization*, WO2006073366 A1, 2006.
60 C. Castel, X. Fernandez, L. Lizzani-Cuelier, C. Perichet and S. Lavoine, *J. Agric. Food Chem.*, 2006, **54**, 5584–8854.
61 T. Kokubo, H. Kushitani, S. Sakka, T. Kitsugi and T. Yamamuro, *J. Biomed. Mater. Res.*, 1990, **24**, 721–734.
62 A. Carado, M. K. Passarelli, J. Kozole, J. E. Wingate, N. Winograd and A. V. Loboda, *Anal. Chem.*, 2008, **80**, 7921–7929.
63 A. Carado, PhD Thesis, The Pennsylvania State University, 2010.